AFRL-AFOSR-VA-TR-2019-0355

Physics-Based-Adaptive Plasma Model for High-Fidelity Numerical Simulations

Uri Shumlak
UNIVERSITY OF WASHINGTON

11/19/2019
Final Report

Air Force Research Laboratory
AF Office Of Scientific Research (AFOSR)/ RTB1
Arlington, Virginia 22203
Air Force Materiel Command

DISTRIBUTION A: Distribution approved for public release.

REPORT DOCUMENTATION PAGE

Form Approved
OMB No. 0704-0188

1. REPORT DATE *(DD-MM-YYYY)*	2. REPORT TYPE	3. DATES COVERED *(From - To)*
21-11-2019	Final Performance	15 Jul 2015 to 14 Aug 2019

4. TITLE AND SUBTITLE
Physics-Based-Adaptive Plasma Model for High-Fidelity Numerical Simulations

5a. CONTRACT NUMBER

5b. GRANT NUMBER
FA9550-15-1-0271

5c. PROGRAM ELEMENT NUMBER
61102F

6. AUTHOR(S)
Uri Shumlak

5d. PROJECT NUMBER

5e. TASK NUMBER

5f. WORK UNIT NUMBER

7. PERFORMING ORGANIZATION NAME(S) AND ADDRESS(ES)
UNIVERSITY OF WASHINGTON
4333 BROOKLYN AVE NE
SEATTLE, WA 98195-0001 US

8. PERFORMING ORGANIZATION REPORT NUMBER

9. SPONSORING/MONITORING AGENCY NAME(S) AND ADDRESS(ES)
AF Office of Scientific Research
875 N. Randolph St. Room 3112
Arlington, VA 22203

10. SPONSOR/MONITOR'S ACRONYM(S)
AFRL/AFOSR RTB1

11. SPONSOR/MONITOR'S REPORT NUMBER(S)
AFRL-AFOSR-VA-TR-2019-0355

12. DISTRIBUTION/AVAILABILITY STATEMENT
A DISTRIBUTION UNLIMITED: PB Public Release

13. SUPPLEMENTARY NOTES

14. ABSTRACT
A physics-based-adaptive plasma model and an appropriate computational algorithm are developed to numerically simulate plasma phenomena in high-fidelity. The plasma model is 'refined' or 'coarsened' based on local physical plasma parameters to provide high fidelity throughout the domain. The plasma model uses continuum representations of the plasma, which include a kinetic description, multi-fluid plasma models (13N-moment and 5N-moment), and single-fluid MHD models. A blended finite element method is developed to implicitly treat the fastest physical phenomena and to explicitly treat the slower physical phenomena. The solution approach provides high-order accuracy and computational efficiency

15. SUBJECT TERMS
Plasma, Simulation, Vlasov, multi-scale, multi-physics, MHD, magneto hydrodynamics, electromagnetic

16. SECURITY CLASSIFICATION OF:			17. LIMITATION OF ABSTRACT	18. NUMBER OF PAGES	19a. NAME OF RESPONSIBLE PERSON
a. REPORT	b. ABSTRACT	c. THIS PAGE			MOSES, JULIE
Unclassified	Unclassified	Unclassified	UU		19b. TELEPHONE NUMBER *(Include area code)* 703-696-9586

Standard Form 298 (Rev. 8/98)
Prescribed by ANSI Std. Z39.18

Final Performance Report (7/15/15 – 8/14/19)

AFOSR Grant No. FA9550-15-1-0271

"PHYSICS-BASED-ADAPTIVE PLASMA MODEL FOR HIGH-FIDELITY NUMERICAL SIMULATIONS"

Submitted to

Dr. Jason Marshall
Program Manager, Plasma and Electroenergetic Physics
Air Force Office of Scientific Research / RTB
875 N. Randolph St.
Arlington, VA 22203

University of Washington
Department of Aeronautics and Astronautics
Aerospace & Energetics Research Program
Box 352400
Seattle, WA 98195-2400

Dr. Uri Shumlak
Principal Investigator

11/12/19

PHYSICS-BASED-ADAPTIVE PLASMA MODEL FOR HIGH-FIDELITY NUMERICAL SIMULATIONS

AFOSR Grant No. FA9550-15-1-0271

U. Shumlak

Department of Aeronautics and Astronautics
Aerospace & Energetics Research Program
University of Washington

Abstract

A physics-based-adaptive plasma model and an appropriate computational algorithm are developed to numerically simulate plasma phenomena in high-fidelity. The plasma model [1] is "refined" or "coarsened" based on the local physical plasma parameters to provide adequate model fidelity throughout the domain at all times of the simulation. The plasma model uses continuum representations of the plasma, which include a kinetic description for the highest fidelity, multi-fluid plasma models ($13N$-moment [2] and $5N$-moment [3]), and single-fluid MHD models for the lowest fidelity. The models include evolution equations for the electromagnetic fields, electron fluid, ion fluid, neutral fluid, and any additional species. The continuum kinetic model is developed in a conservative form [4] that exploits geometric symmetries of the physical domain. The large mass difference between electrons and ions introduces disparate time and spatial scales and requires a numerical algorithm with sufficient accuracy to capture the multiple scales. In addition, the characteristic timescales for the electromagnetic fields is much shorter than the timescales of the ion and neutral fluids, so a blended finite element method [5] is developed to implicitly treat the fastest physical phenomena (electron fluid and electromagnetic field evolution) and to explicitly treat the slower physical phenomena (ion and neutral fluid evolution). The solution approach provides high-order accuracy and computational efficiency.

1 Project Description

Many existing and emerging technologies that are important to the U. S. Air Force, industry, and general science rely on plasmas and plasma applications. These applications include high power microwave devices, plasma actuation of airstreams, drag reduction for hypersonic vehicles, advanced space propulsion, weapons effects simulations, radiation production from fusion, etc. Advancing plasma technologies requires a fundamental and accurate understanding of the underlying physical effects and the

resulting plasma dynamics. Plasma dynamics inherently involve complex physical phenomena because the dynamics are affected by short-range (collisions) and long-range (electromagnetic fields) forces. The great utility of plasmas stems from these multi-scale forces. In general, plasmas fall into a density regime where they exhibit both collective (fluid) behavior and individual (particle) behavior. The intermediate regime complicates the analytical and computational modeling of plasmas. Accurate numerical simulations requires high-fidelity plasma models and innovative numerical algorithms that are tuned to solve the specific physical models that capture the multi-scale and multi-physics phenomena that are present in plasmas. Developing a physics-based-adaptive plasma model facilitates high-fidelity numerical simulations while making efficient use of the available computational resources.

This final technical report describes the primary research accomplishments performed during this project. The accomplishments include developing consitituent plasma models of varying degrees of fidelity: multi-species continuum kinetic plasma model [4], multi-fluid plasma models ($13N$-moment [2] and $5N$-moment [3]), and single-fluid MHD models for the lowest fidelity. Novel and efficient methods to spatially discretize and temporally advance the governing equations were also developed, such as the blended finite element method [5]. Initial investigations were performed to couple the constituent plasma models into a domain-hybridized plasma model [1]. This report highlights the research, which are described in more detail in the associated journal publications.

1.1 Continuum Plasma Models

Plasma behavior prediction and understanding have been significantly advanced through the development of reduced plasma models and their numerical solution. The most complete continuum model for plasma is described using kinetic theory where each species α of a plasma is described by a time-dependent distribution function $f_\alpha(\mathbf{x}, \mathbf{v}, t)$ in physical and velocity space. The evolution of the distribution functions is described by the Boltzmann equation

$$\frac{\partial f_\alpha}{\partial t} + \mathbf{v} \cdot \frac{\partial f_\alpha}{\partial \mathbf{x}} + \frac{q_\alpha}{m_\alpha} \left(\mathbf{E} + \mathbf{v} \times \mathbf{B} \right) \cdot \frac{\partial f_\alpha}{\partial \mathbf{v}} = \left. \frac{\partial f_\alpha}{\partial t} \right|_c . \tag{1}$$

The plasma is composed of ion and electron species and possibly additional species for neutrals or impurity ions.

The Boltzmann equation coupled with Maxwell's equations for electromagnetic fields completely describe the plasma dynamics. Plasmas have been simulated using this model with specific forms of the collision operator (e.g. Vlasov equation and Fokker-Planck equation). [4,6–16] However, the Boltzmann equation spans six dimensions corresponding to spatial position and velocity, in addtion to time. As a consequence of the large dimensionality plasmas are simulated using the Boltzmann equation only when required to capture the essential physics. The applications are generally limited to plasmas with narrow distributions, small spatial extent, and short time durations.

The continuum kinetic model is implemented on a mixed structured/unstructured phase space finite element mesh to be able to handle complex physical space geometry while maintaining the computational efficiency of a rectilinear mesh in velocity space.

Formulating Eq. (1) in conservation form has been shown [16] to improve the numerical properties of the solutions. An outcome of the present research project expands on this concept for axisymmetric geometries [4]. The performance is demonstrated through analysis of benchmark problems.

Particle in cell (PIC) plasma models apply the Boltzmann equation to representative superparticles, which are far fewer than the number of particles in the actual plasma. [17] In this manner, PIC methods provide a statistical sampling of phase space. While PIC methods have been successful in modeling many physical effects [18–20], they are not universally applicable due to grid effects and statistical errors or particle noise, which scales with the number of particles as $N^{-1/2}$ [21]. PIC simulations have similar limitations as simulations using kinetic theory.

The particle in cell (PIC) plasma models have successfully solved the Boltzmann equation with representative superparticles, which are far fewer than the number of particles in the actual plasma [17]. However, PIC methods are not universally applicable due to grid effects and statistical errors or particle noise, which scales with the number of particles as $N^{-1/2}$ [21]. Another approach to capture more complete physics is to generalize the single-fluid MHD model that results from moments of the Boltzmann equation, Eq. (1). The generalization described here allows for multiple species, and the resulting model is the multi-fluid plasma model. Assumptions about the lowest-order velocity distribution function determines the number of moments that must be evolved: five moments for perturbations about a Maxwellian distribution and thirteen moments for perturbations about a Pearson-type-IV distribution [2, 22]. Furthermore, the moment equations can include higher moments to more accurately model the evolution of plasmas that deviate from thermodynamic equilibrium.

1.1.1 Moment Method to Yield Fluid Plasma Models

Moments of the Boltzmann equation, Eq. (1), provide equations that govern the evolution of the moment variables. The moment variables are defined from moments of the distribution function. For example,

$$n_\alpha = \int f_\alpha(\mathbf{v}) d\mathbf{v}, \tag{2}$$

$$n_\alpha u_{\alpha_i} = \int v_i f_\alpha(\mathbf{v}) d\mathbf{v}, \tag{3}$$

$$\vdots$$

where the integrals are performed over all velocity space and i represents the spatial coordinate index. The resulting fluid variables are number density n_α, velocity u_{α_i}, etc. Moments of the Boltzmann equation provide evolution equations for these moment

variables. The governing equations for the limiting case of a collisionless plasma with only two species, ions and electrons, the two-fluid plasma model is presented in Ref. [23].

The governing equations of the two-fluid plasma model can be combined to form the single-fluid MHD model [24]. In the derivation of the MHD model several approximations are made, which limit its applicability to low frequency phenomena and ignores potentially significant finite electron mass and charge separation effects. These limitations are not present in the multi-fluid plasma model.

Generalizing the moment approach to include an arbitrary number of species and to include atomic reactions yields the multi-fluid plasma model. The derivation follows that presented, for example, by Braginskii in Ref. [25]. However, the form of the equations are derived here for the conservation variables in flux/source form where hyperbolic and parabolic fluxes are in balance with source terms. The equation systems can be expressed as

$$\frac{\partial}{\partial t} q_\alpha + \frac{\partial}{\partial x_k} F_{\alpha_k} = S_\alpha, \tag{4}$$

where q_α is the vector of conservation variables of species α, $\mathbf{F}_\alpha$ is the tensor of hyperbolic fluxes for α, and S_α is the source vector for α. Note that throughout this proposal vectors and tensors are represented in bold, and their components are represented in italics with subscript indices (i, j, k, l). Repeated indices of the spatial coordinate are summed in the usual convention of Einstein notation. The source vector includes the coupling to the other fluid species and to the electromagnetic fields. For example, the electric and magnetic fields appear in the source terms of any charged-fluid equations. The field dynamics are governed by Maxwell's equations, which have source terms that contain the charged-fluid variables. See Sec. **??**. Maxwell's equations can be expressed in the form given by Eq. (4) where $\alpha = EM$.

Since each evolution equation derived from the moment approach introduces the next higher moment, the series continues indefinitely. The equation system must be terminated and closure relations must be specified that relate the higher moment variables to the lower moment variables in the system. The complete multi-fluid model and its extensions are presented in Sec. 1.1.2.

1.1.2 The 5N-Moment Multi-Fluid Plasma Model

The governing equations for multi-fluid plasma models are derived by taking moments of the Boltzmann equation, Eq. (1), for each species, as briefly introduced in Sec. 1.1.1. The multi-fluid plasma model (including the electromagnetic equations) are expressed in divergence form as in Eq. (4). Each fluid is assumed to be sufficiently close to thermodynamic equilibrium that its velocity distribution function is well approximated by a limited expansion about a Maxwellian distribution. The fluid variables are derived

by taking moments of the distribution function.

$$\rho_\alpha = m_\alpha \int f_\alpha(\mathbf{v}) d\mathbf{v}, \tag{5}$$

$$\rho_\alpha u_{\alpha_i} = m_\alpha \int v_i f_\alpha(\mathbf{v}) d\mathbf{v}, \tag{6}$$

$$p_\alpha = \rho_\alpha T_\alpha = m_\alpha \int \frac{1}{3}\mathbf{w}^2 f_\alpha(\mathbf{w}) d\mathbf{w}, \tag{7}$$

where m_α is the mass of species α, and the distribution function is expressed equivalently as a function of either the velocity $\mathbf{v}$ or the random velocity about the mean fluid velocity $\mathbf{w} = \mathbf{v} - \mathbf{u}_\alpha$. The fluid variables for each species are mass density ρ_α (1 component), velocity $\mathbf{u}_\alpha$ (3 components), and pressure p_α (1 component). T_α is the temperature associated with species α. The model has a total of five fluid variables or components for each species and is called the $5N$-moment fluid model.

An evolution equation for the mass density of each species is given by the zeroth moment of the Boltzmann equation.

$$\frac{\partial}{\partial t}\rho_\alpha + \frac{\partial}{\partial x_k}\left(\rho_\alpha u_{\alpha_k}\right) = \left.\frac{\partial}{\partial t}\rho_\alpha\right|_\Gamma \tag{8}$$

The net mass production rate of species α due to atomic reactions is denoted on the right-hand side of the equation with a subscript Γ. Contributions due to atomic reactions are described later in Sec. **??**.

The first moment of the Boltzmann equation yields momentum equations and describes the evolution of the momentum density for each species.

$$\frac{\partial}{\partial t}\left(\rho_\alpha u_{\alpha_i}\right) + \frac{\partial}{\partial x_k}\left(\rho_\alpha u_{\alpha_i} u_{\alpha_k} + p_\alpha I_{ik}\right) = q_\alpha n_\alpha \left(E_i + \epsilon_{ijk} u_{\alpha_j} B_k\right) - \sum_\beta R_{\alpha\beta_i} + \left.\frac{\partial}{\partial t}\left(\rho_\alpha u_{\alpha_i}\right)\right|_\Gamma \tag{9}$$

where $\mathbf{E}$ and $\mathbf{B}$ are the electric and magnetic fields and $\mathbf{R}_{\alpha\beta}$ is the momentum transfer vector from species α to species β due to collisions. $\mathbf{I}$ is the identity tensor. The number density has been introduced and is defined by $n_\alpha \equiv \rho_\alpha / m_\alpha$. The net momentum production rate of species α due to atomic reactions is denoted on the right-hand side of the equation with a subscript Γ.

The second moment of the Boltzmann equation yields an energy equation for each species, which is expressed in divergence form for the total energy.

$$\frac{\partial}{\partial t}\varepsilon_\alpha + \frac{\partial}{\partial x_k}\left[\left(\varepsilon_\alpha + p_\alpha\right) u_{\alpha_k} + h_{\alpha_k}\right] = q_\alpha n_\alpha u_{\alpha_j} E_j + \sum_\beta u_{\alpha_j} R_{\alpha\beta_j} + \sum_\beta Q_{\alpha\beta} + + \left.\frac{\partial}{\partial t}\varepsilon_\alpha\right|_\Gamma \tag{10}$$

where $\mathbf{h}_\alpha$ is the heat flux vector, $Q_{\alpha\beta}$ is the heat generated in species α due to collisions with species β, and the total energy is defined by

$$\varepsilon_\alpha \equiv \frac{1}{\gamma - 1} p_\alpha + \frac{1}{2}\rho_\alpha u_{\alpha_j}^2 \tag{11}$$

and γ is the ratio of specific heats. The evolution equation for the total energy can be combined with the previous two moment equations to provide an expression for the evolution of pressure. The energy addition rate of species α due to atomic reactions is denoted on the right-hand side of the equation with a subscript Γ.

Since the heat flux represents a higher moment of the distribution function, a closure relation must be specified that relates it to the lower moment variables. Fourier's law is a commonly used relation, which gives the i^{th} component of the heat flux as

$$h_{\alpha_i} = -\kappa_{\alpha_{ij}} \frac{\partial}{\partial x_j} T_\alpha, \tag{12}$$

where $\kappa_{\alpha_{ij}}$ is the ij component of the thermal conductivity tensor which, in general, depends on the strength and relative orientation of the magnetic field. Additional closure relations are needed if a pressure tensor is used instead of the scalar pressure used in the momentum and energy evolution equations.

The $5N$-moment model and appropriate closures are derived using a Chapman-Enskog expansion of the distribution function. The distribution function is assumed to be a Maxwellian (thermodynamic equilibrium) distribution with an expansion in powers of a small parameter given by the Knudsen number, the ratio of the mean free path to the characteristic plasma size. Closure relations for the transport coefficients are found by retaining only the linear terms of the expansion. For examples of calculations of transport coefficients, see Ref. [25, 26].

The electromagnetic fields influence the motion of the plasma fluid through the Lorentz force, which appears in all plasma models. The motion of the plasma influences the evolution of the electromagnetic fields through the redistribution of charge density and current density. Maxwell's equations govern the evolution of the electromagnetic fields. The net charge density and total current density are calculated directly from the plasma state, i.e. the distribution functions or the multi-fluid plasma variables, as

$$\rho_c = \sum_\alpha q_\alpha n_\alpha = \sum_\alpha q_\alpha \int f_\alpha(\mathbf{v}) d\mathbf{v} \tag{13}$$

$$j_i = \sum_\alpha q_\alpha n_\alpha u_{\alpha_i} = \sum_\alpha q_\alpha \int v_i f_\alpha(\mathbf{v}) d\mathbf{v}. \tag{14}$$

These terms appear as source terms in Maxwell's equations, which can be expressed as

$$\frac{\partial}{\partial t} B_i = -\epsilon_{ijk} \frac{\partial}{\partial x_j} E_k \tag{15}$$

$$\epsilon_0 \mu_0 \frac{\partial}{\partial t} E_i = \epsilon_{ijk} \frac{\partial}{\partial x_j} B_k - \mu_0 j_i \tag{16}$$

$$\tag{17}$$

Mathematically, if the initial fields satisfy the divergence constraints, then the field evolution maintains the constraints. Numerically, the divergence constraints must be

explicitly enforced by "cleaning" the fields with either an elliptic method [27], a hyperbolic method [28], or a parabolic method [29].

The Jacobians of the hyperbolic fluxes $\partial \mathbf{F}_\alpha / \partial q_\alpha$ of the governing equations are constructed in the usual way from Eq. (4). The eigenvalues of the flux Jacobians give the characteristic velocities. In one dimension, the eigenvalues of the fluid equations are

$$\lambda_{fluid} = \{v_{\alpha_x}, v_{\alpha_x} \pm c_{s_\alpha}\} \tag{18}$$

where the acoustic speed for species α is defined as

$$c_{s_\alpha} = \sqrt{\frac{\gamma T_\alpha}{m_\alpha}}. \tag{19}$$

The electron acoustic speed is larger than the ion acoustic speed for the same fluid temperatures due to the large ion to electron mass ratio. The electron acoustic speed can be larger than the Alfvén speed, which is a component of the eigenvalues of MHD. The Alfvén speed for an ion/electron plasma is defined as

$$v_A = \frac{B}{\sqrt{\mu_0 \left(m_i n_i + m_e n_e\right)}} \tag{20}$$

where B is the magnitude of the magnetic field and μ_0 is the permeability of free space ($4\pi \times 10^{-7}$ H/m). The eigenvalues of the field equations are

$$\lambda_{field} = \{\pm c\}, \tag{21}$$

where c is the speed of light. Therefore, the eigenvalues of the multi-fluid plasma model are generally not bounded by the eigenvalues of the MHD model. In general, the fastest times that must be resolved in the multi-fluid plasma model are the timescales associated with the electromagnetic fields and the electron fluid, namely, the light transit time and the electron plasma oscillation period.

1.1.3 The 13N-Moment Multi-Fluid Plasma Model

The 5N-moment multi-fluid plasma model presented above provides an adequate description for many plasmas that remain sufficiently close to thermodynamic equilibrium. For truly non-equilibrium plasmas, the kinetic model described at the beginning of Sec. 1.1 is needed. Generalizations of the moment method (higher moment models) extend the applicability of fluid models to non-equilibrium plasmas. The higher moments extend the ability to characterize the distribution function with averaged or moment variables.

The 13N-moment multi-fluid plasma model provides a logical extension of the 5N-moment plasma model. The model as first introduced by Grad [30] and has since been refined by many others, for example Refs. [2, 22, 31–34]. Specifically, Ref. [22] provides a derivation for gas dynamics using a Pearson-type-IV distribution for the velocity

distribution function that better matches experimental measurements and improves the hyperbolicity of the resulting evolution equations. These are important advantages over Grad's initial method. The results are only briefly presented here for a neutral gas. We have extend the model to derive a $13N$-moment fluid model for a multicomponent plasma.

As before, moments of the distribution function provide the fundamental fluid variables. Consistent with the original derivation by Grad [30], only the variables with an explicit physical meaning are retained. For each species fluid the density and velocity is defined as in Eqs. (5) and (6). The scalar pressure is replaced with the pressure tensor and the heat flux vector is also defined as a solution variable. These variables are defined as

$$p_{ij} = m \int w_i w_j f(\mathbf{w}) d\mathbf{w}, \tag{22}$$

$$h_i = m \int \frac{1}{2} \mathbf{w}^2 w_i f(\mathbf{w}) d\mathbf{w}, \tag{23}$$

where the species subscript α has been dropped for clarity. In addition to the 4 components of density and velocity, the model has a total of thirteen fluid variables or components for each fluid. The pressure tensor $\mathbf{p}$ has 6 components, since $p_{ij} = p_{ji}$ and heat flux $\mathbf{h}$ has 3 components. Note the scalar pressure is the trace of the pressure tensor, and is given by

$$p = \rho T = m \int \frac{1}{3} \mathbf{w}^2 f(\mathbf{w}) d\mathbf{w}, \tag{24}$$

which is consistent with the definition from Eq. (7).

Taking moments of the Boltzmann equation provides the evolution equations for the moment variables.

$$\frac{\partial}{\partial t}\rho + \frac{\partial}{\partial x_k}\left(\rho u_k\right) = 0, \tag{25}$$

$$\frac{\partial}{\partial t}\left(\rho u_i\right) + \frac{\partial}{\partial x_k}\left(\rho u_i u_k + p_{ik}\right) = 0, \tag{26}$$

$$\frac{\partial}{\partial t}\left(\rho u_i u_j + p_{ij}\right) + \frac{\partial}{\partial x_k}\left(\rho u_i u_j u_k + 3 p_{ij} u_k + m_{ijk}\right) = 0, \tag{27}$$

$$\frac{\partial}{\partial t}\left[\frac{\rho u_j^2 + p_{jj}}{2} u_i + p_{ij} u_j + h_i\right] + \frac{\partial}{\partial x_k}\left[\frac{\rho u_j^2 + p_{jj}}{2} u_i u_k + \frac{p_{ik} u_j^2}{2} + 2 u_i p_{jk} u_j + 2 h_i u_k + m_{ijk} u_j + \frac{R_{ik}}{2}\right] = 0. \tag{28}$$

Equations (27) and (28) provide evolution equations for the pressure tensor and heat flux vector. The equation system must be closed for the variables corresponding to the higher moments, namely,

$$m_{ijk} = m \int w_i w_j w_k f(\mathbf{w}) d\mathbf{w}, \tag{29}$$

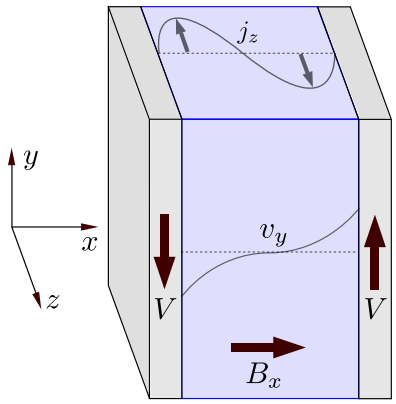

Figure 1: Hartmann flow diagram showing geometry of shear flow and imposed magnetic field as well as the resultant current density.

$$R_{ij} = m \int \mathbf{w}^2 w_i w_j f(\mathbf{w}) d\mathbf{w}. \tag{30}$$

Closure relations are derived by assuming a particular form of the distribution function. For the proposed work, a Pearson-type-IV distribution will be used, as in Ref. [22]. A more complete description of the $13N$-moment multi-fluid plasma model that was developed for this research project is described in Ref. [2].

Benchmarking magnetized plasma transport in moderately collisional systems is a difficult process, and few test problems exist. The Hartmann flow problem is a classic benchmark [35] for resistive, viscous MHD models near the highly collisional regime. The multi-species Hartmann flow, discussed and derived in Ref. [2], is an extension of the single-fluid MHD problem.

Similar to a Couette flow, the Hartmann flow problem, shown in Fig. 1, uses two infinite conducting plates to drive shear flow along the y-direction. The shear, along with an imposed magnetic field along x drives a current in the z-direction which is balanced by resistive forces. The flow generated along z interacts with B_x to drive a force along y, suppressing, or flattening, the viscous boundary layer.

A viable parameter space for this simulation is $\nu_p\tau = 100$, $\omega_c\tau = 4$, $\omega_p\tau = 100$, wall velocity $V = 10^{-3}$, and a domain of $L = 1$. The low wall velocity reduces the viscous and resistive heating, while the relatively low magnetization ($\omega_c \ll \nu_p$) reduces the anisotropic magnetization effects that the analytical form ignores. A small $\omega_p\tau$ allows for a larger time step. The fluid is initialized in thermal equilibrium with $n_\alpha = T_\alpha = B_x = 1$ and $v_y^\alpha = 2Vx$, for $x \in [-0.5, 0.5]$. All other electric and magnetic fields are initialized to zero. The boundary conditions are no-slip, adiabatic, conducting walls.

The results shown in Fig. 2 are for a two-species plasma with masses $A_\alpha = \{10^{-2}, 1\}$, charges $Z_\alpha = \{-1, 1\}$, and speed of light $(c/v_0) = 100$ after a normalized time of $t = 10$. The $13N$-moment plasma model is solved without diffusive stabilization and

is shown to capture the viscous boundary layer of the Couette flow, as well as the flattening of the internal shear profile due to the magnetic forces. The test case has shown that at moderate to high collisionalities and low magnetization, the two-fluid 13-moment plasma model is consistent with the two-fluid $5N$-moment plasma model. The numerical results agree closely to the analytical solutions.

1.2 Computational Solution Framework: WARPXM

Our Computational Plasma Dynamics Group at the University of Washington has developed accurate numerical algorithms for the two-fluid plasma model that are based on finite volume [23, 36] and DG methods [3, 37–39]. Higher moment plasma models ($10N$ and $13N$) have been derived and investigated [2, 32–34]. Numerical formulations have been investigated that allow for the implicit solutions of plasma models [35], including the blended finite element method [5]. These computational advances have been applied to study plasma phenomena with high fidelity models, e.g. Refs. [40–42]. In addition, we have developed non-reflecting open boundary conditions that allow simulating infinite space on finite domains [43, 44].

Developments of FE methods applied to continuum plasma models is the focus of the current research project. The algorithm research and development have been implemented in a flexible software framework called WARPXM (Washington Approximate Riemann Plasma) [3, 39, 42], which uses C++ object oriented programming and other modern software techniques to simplify the maintainability and extensibility of the code and HDF5 for parallel output. WARPXM uses MPI message passing for parallel computer architectures.

1.2.1 The Blended Finite Element Method

The blended finite element method uses an implicit-explicit to solve the multi-fluid plasma model and Maxwell's equations by splitting the governing equation system to according to the expected physics. The spatial representation for all of the system variables is based on finite element methods where the simulation domain is divided into discrete elements, which are either quadrilaterals (2D) or hexahedrals (3D). The variation of the solution variables within each element are modeled by projecting the variables onto a set of spatially dependent basis functions v_h of order h, such that within each element Ω variable q is represented as

$$q_\Omega(\mathbf{x}) = \sum_h q_{\Omega_h} v_h(\mathbf{x}). \tag{31}$$

The basis functions are Legendre polynomials or Jacobi polynomials for the proposed implementation. The finite element representation captures high-order spatial variations, which is critical when anisotropic properties exist [45] or when hyperbolic fluxes are balanced by the fluxes from other species, which occurs at equilibrium.

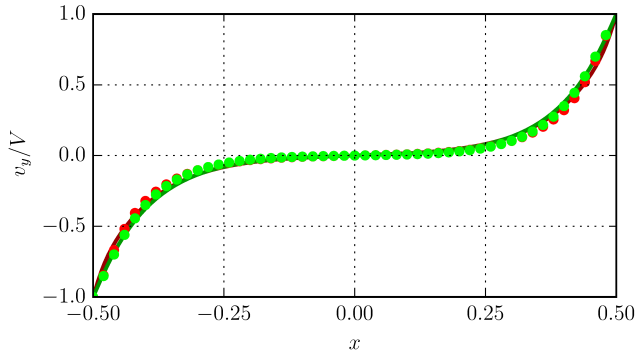

(a)

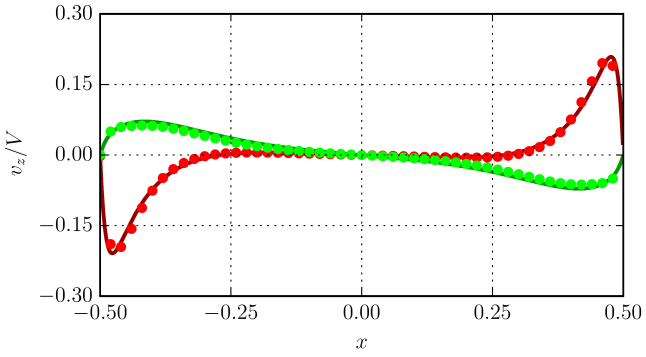

(b)

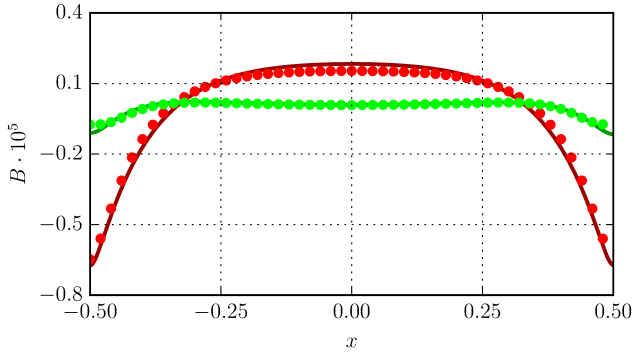

(c)

Figure 2: Comparison of $13N$-moment plasma model solutions (dots) to analytical solutions (lines) for a two-fluid Hartmann flow. (a) In-plane velocity and (b) out-of-plane velocity for species $A_0 = 10^{-2}$, $Z_0 = -1$ (red) and $A_1 = 1$, $Z_1 = 1$ (green). (c) Magnetic fields B_y (red) and B_z (green). Results show good agreement between the numerical and analytical solutions.

The governing equations for the multi-fluid plasma model can be expressed as given by Eq. (4). The equations can be grouped according to their physically characteristic spatial and temporal scales, which forms the basis for selecting the appropriate computational method. The fast temporal and short spatial dynamics of the electron fluid and electromagnetic fields suggests solving these governing equations in a coupled manner as

$$\frac{\partial}{\partial t}\begin{bmatrix} q_{EM} \\ q_e \end{bmatrix} + \frac{\partial}{\partial x_k}\begin{bmatrix} F_{EM_k} \\ F_{e_k} \end{bmatrix} = \begin{bmatrix} S_{EM} \\ S_e \end{bmatrix}, \tag{32}$$

where the source terms, in general, depend on the solution variables of the fields and other species, $S_\alpha = S_\alpha\left(q_{EM}, q_e, q_i, q_n\right)$. The slow temporal and long spatial dynamics of the ion and neutral fluids suggests solving these governing equations in a separately coupled manner as

$$\frac{\partial}{\partial t}\begin{bmatrix} q_i \\ q_n \end{bmatrix} + \frac{\partial}{\partial x_k}\begin{bmatrix} F_{i_k} \\ F_{n_k} \end{bmatrix} = \begin{bmatrix} S_i \\ S_n \end{bmatrix}, \tag{33}$$

where the source terms again, in general, depend on the solution variables of the fields and other species.

A Galerkin method is used to obtain spatially discretized equations. The governing equations are multiplied by each basis function and integrated over the element volume to give the integral equation

$$\int_\Omega v_h \frac{\partial q}{\partial t} dV + \oint_{\partial\Omega} v_h F_k dA_k - \int_\Omega F_k \frac{\partial}{\partial x_k} v_h dV = \int_\Omega v_h S dV. \tag{34}$$

The integrals are evaluated by Gaussian quadrature. The source terms are also projected onto the basis functions, similar to Eq. (31). The solution of Eq. (34) throughout the spatial domain and its time advance provides the complete time-dependent solution. Both the spatial representation and time advance are optimized based on the expected physics. The details of the blended finite element method are described in Ref. [5].

1.3 Domain-Hybridized Plasma Model

Spatial coupling of multiple plasma models [1] offers the potential to minimize the computational cost for the required degree of physical fidelity throughout the domain. The investigation is performed using a high-order discontinuous Galerkin finite element method [37, 38, 46], specifically involving the continuum kinetic multi-species plasma model, $5N$-moment multi-fluid plasma model, and magnetohydrodynamics (MHD) models, implemented in WARPXM. It is demonstrated that transition mixing layers do not necessarily guarantee conservation of important physical quantities such as mass, momentum, or energy. Nevertheless, coupling between the models can be performed consistently. Two such numerical fluxes are derived, of which one flux is consistent with the MHD and two-fluid plasma models, and a second flux guarantees conservation properties but without a consistent definition of the underlying variables.

1.3.1 5N-Moment to MHD

A two-dimensional planar plasma opening switch is implemented to test the direct variable translation method for coupling two-fluid and MHD. Five different domain subdivisions are tested:

(a) Uniform MHD: A single MHD plasma model is used in the entire domain.

(b) Uniform two-fluid: A two-fluid plasma model is used in the entire domain.

(c) Mixed.25: A two-fluid model is used in the region $x \in [0, 0.25]$, and an MHD model is used in the region $x \in [0.25, 1]$.

(d) Mixed.5: A two-fluid model plasma model is used in the region $x \in [0, 0.5]$, and an MHD model is used in the region $x \in [0.5, 1]$.

(e) Adaptive: Uses the subdivision Mixed.25 for $t \in [0, 0.8]$, then switches to Mixed.5 for $t \geq 0.8$.

The temporal domain is discretized using Heun's method [47]. A high density slab of plasma is initialized with a notch perturbation in the middle. This configuration is shown in Fig. **??**. The plasma is accelerated to the right by imposing $B_z = 1$ on the left boundary. This drives a current in the plasma, producing a Lorentz force. The testing parameters used are:

$$\omega_p \tau = 2000 \tag{35}$$

$$\frac{\delta_p}{L} = 10^{-2} \tag{36}$$

$$Z_i = -Z_e = 1 \tag{37}$$

$$A_i = 100 A_e = 1 \tag{38}$$

$$\gamma = \frac{5}{3} \tag{39}$$

$$P_i = P_e = \frac{1}{2} \tag{40}$$

Figure 3 shows the plasma density at $t = 1$, shortly after the adaptive method has remapped the domain. An instability begins developing around where the initial perturbation was in all cases except for the uniform MHD case. At $t = 2$, Fig. 4 shows that the adaptive case is capable of matching the fine-scale instability structure of the Uniform two-fluid and Mixed.5 cases. However, the instabilities which developed on the two-fluid side of the Mixed.25 case balloons on the MHD side and loses the fine-scale structure. This is especially prevalent at $t = 2.5$ in Fig. 5. At this point the adaptive case is still capable of maintaining fine-scale instability structures on the trailing edge of the bulk plasma; however, the leading edge does not have similar instability structures as the Uniform two-fluid and Mixed.5 cases. It is suspected that this is due to the leading edge being on the MHD side initially before the adaptive method moves the model interface ahead of the leading edge.

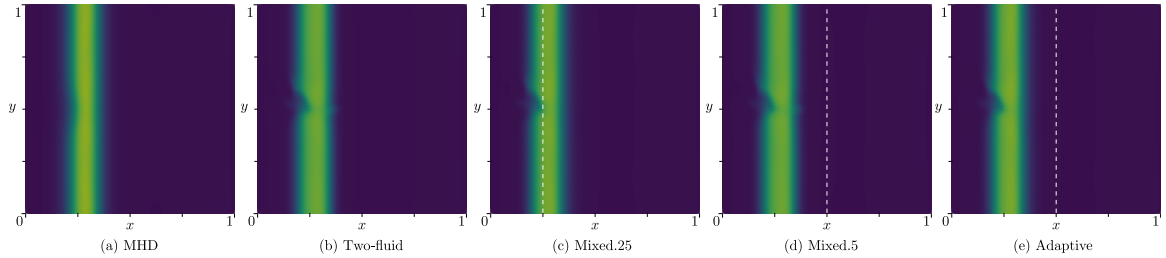

Figure 3: Planar plasma switch density at $t = 1$. The adaptive method has re-partitioned the domain variables. An instability at the density perturbation starts developing in all models except for the Uniform MHD case.

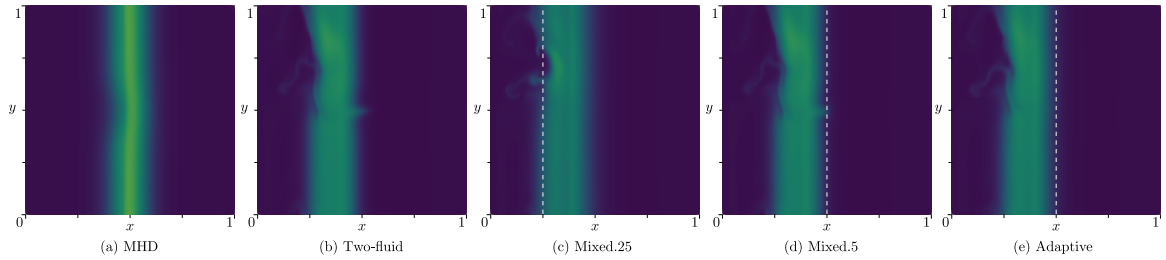

Figure 4: Planar plasma switch density at $t = 2$. The bulk plasma has transitioned past $x = 0.25$ for all models. Some instabilities which have developed in the two-fluid region of the Mixed.25 case balloon on the MHD side, unlike the Uniform two-fluid or Mixed.5 cases. The adaptive method maintains similar instability structures as the Uniform two-fluid and Mixed.5 cases.

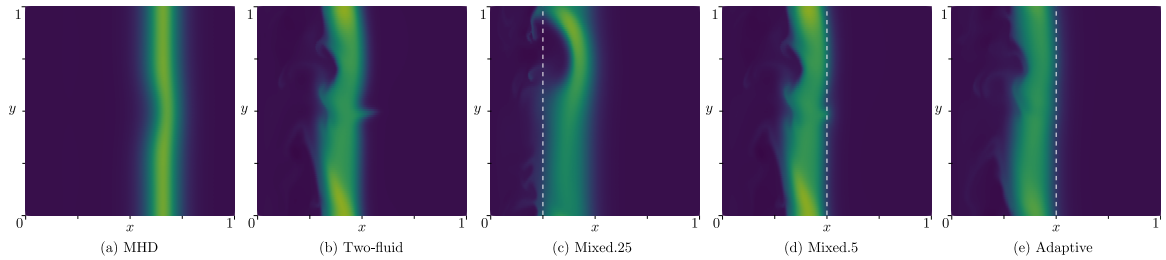

Figure 5: Planar plasma switch density at $t = 2.5$. Ballooning of the instability in the Mixed.25 case is significant. The adaptive case maintains most of the fine-scale structure found in the Uniform two-fluid and Mixed.5 cases on the trailing edge, however the leading edge has noticeable differences.

The test cases have been run with a few different fixed timesteps using identical initial conditions. No new numerical instabilities which result from coupling the models when the coupling assumptions are well matched was noticed. Stability appears to be limited by the limits of the constituent models used. Additional stabilization mechanisms such as artificial viscosity or limiters were not needed for this particular problem.

1.4 Continuum Kinetic to $5N$-Moment

Investigations of spatial coupling of the continuum kinetic and $5N$-moment multi-fluid plasma models have also been investigated by simulating a wall-bounded two-species plasma.

The continuum kinetic model is used to solve this problem as described in Ref. [48] with a domain of $x \in [-128\lambda_D, 128\lambda_D]$ with 256 elements. The outer 32 elements from both left and right are solved using the Vlasov-Maxwell system for ion and electron distributions while the interior elements are solved with the $5N$-moment model for fluid ions and electrons. A realistic mass ratio is used, such that $A_i = 1$, $A_e = 1/1836$, with charges $Z_i = +1$, $Z_e = -1$. Phase space is spans $v_\mathrm{i} \in [-6v_{\mathrm{th_i}}, +6v_{\mathrm{th_i}}]$ and $v_\mathrm{i} \in [-6v_{\mathrm{th_e}}, +6v_{\mathrm{th_e}}]$ for ions and electrons, respectively, using 48 square elements for each physical element and as with the double rarefaction waves problem, first order polynomials and second order timestepping is used.

Simulation results comparing moments for the ion fluid are shown in Fig. 6. For comparison, a full kinetic simulation is also performed (dashed black lines). The ion phase space is shown in Fig. 7. The solutions for the domain-hybridized plasma model and for the full kinetic model match closely until the electrons (not shown) deviate significantly from a Maxwellian distribution at model boundaries. However, as long as the $5N$-moment plasma model is physically valid at the model interface, i.e. the distribution functions remain Maxwellian, the domain-hybridized plasma model produces accurate results with reduced computational effort. To simulate this particular problem longer in time, one might choose to move the model boundary farther into the middle portion of the domain where the electron distribution remains closer to a Maxwellian, or to solve the electrons with a full kinetic model while solving the ions with the hybrid approach, which would still reduce the computational effort. The boundary may also be moved dynamically during a simulation using a metric determining the departure of the distribution from a Maxwellian.

2 Project Personnel

This project was performed by Prof. Uri Shumlak, Dr. Eric Meier and graduate students Daniel Crews, Iman Datta, Andrew Ho, Sean Miller, Noah Reddell, Eder Sousa, and Whitney Thomas. Archival journal and conference papers were published reporting on the work from this project:

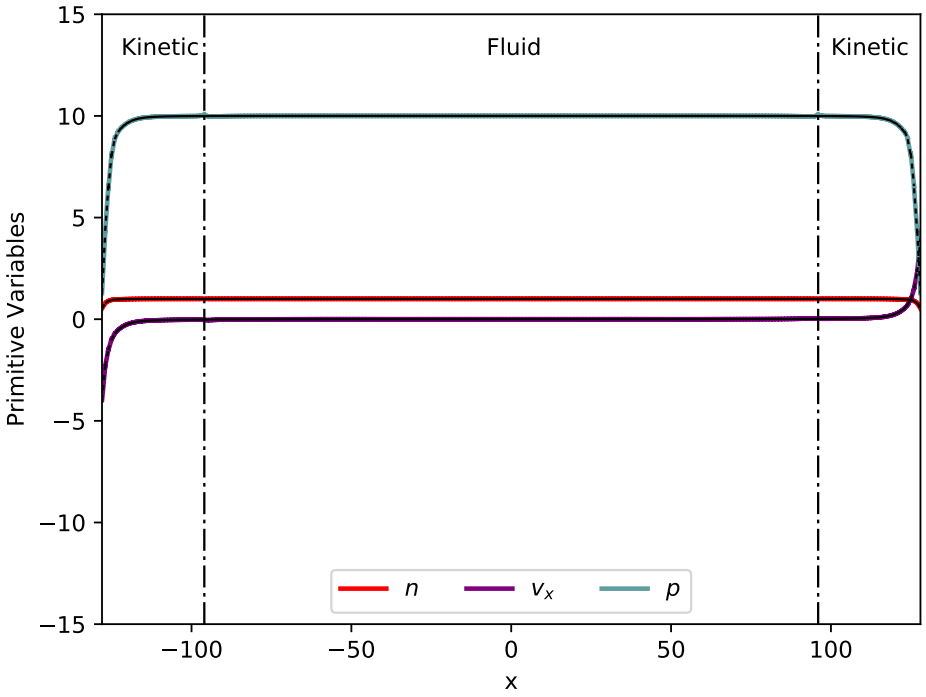

Figure 6: Ion sheath density, velocity, and pressure moments at $t = 20/\omega_{p_e}$ with direct variable translation. The middle domain is solved using the $5N$-moment two-fluid plasma model while the left and right domains are solved using the continuum kinetic two-species plasma model. Simulation results from applying the continuum kinetic model for the entire domain are plotted in black dashed lines for comparison.

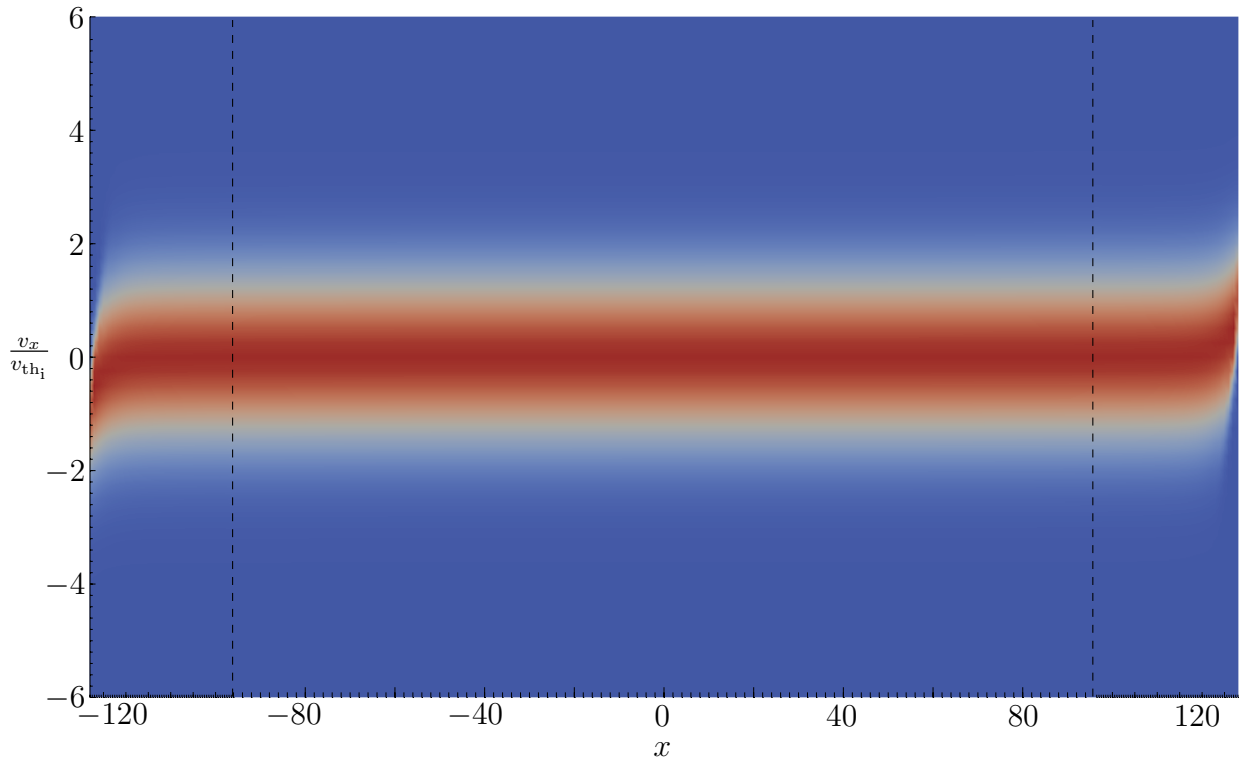

Figure 7: Contours of the ion distribution function at $t = 20/\omega_{p_e}$ solved using the domain-hybridized plasma model. The left and right subdomains $x \in [-128, -96]$ and $x \in [96, 128]$ are modeled with the continuum kinetic two-species plasma model, and the middle subdomain x $\in [-96, 96]$ is modeled with the $5N$-moment two-fluid plasma model.

- A. Ho, I.A.M. Datta, and U. Shumlak. "Physics-Based-Adaptive Plasma Model for High-Fidelity Numerical Simulations." *Frontiers in Physics* **6**, 105 (2018).
- G.V. Vogman, U. Shumlak, and P. Colella. "Conservative fourth-order finite-volume Vlasov–Poisson solver for axisymmetric plasmas in cylindrical (r, v_r, v_θ) phase space coordinates." *Journal of Computational Physics* **373**, 877 (2018).
- S.T. Miller and U. Shumlak. "A multi-species 13-moment model for moderately collisional plasmas." *Physics of Plasmas* **23**, 082303 (2016).
- E.M. Sousa and U. Shumlak. "A blended continuous–discontinuous finite element method for solving the multi-fluid plasma model." *Journal of Computational Physics* **326**, 56 (2016).
- E.M. Sousa, G. Lin, and U. Shumlak. "Uncertainty quantification of the GEM challenge magnetic reconnection problem using the multilevel Monte Carlo method." *International Journal for Uncertainty Quantification* **5**, 327 (2015).

Dissertations and theses can be obtained from the University of Washington library system or from the project website, http://www.aa.washington.edu/research/cpdlab/. Archival publications can be downloaded from ResearchGate.

3 Conclusions

Simulating complicated plasma physics phenomena that are not captured in simpler models requires the simultaneous development of high-fidelity plasma models that can be adapted to the local plasma conditions and robust numerical algorithms that provide high accuracy solutions. The multi-fluid plasma model is proving to be a model that is significantly more advanced and complete than the usual MHD model. Simulations based on the multi-species continuum kinetic represent the highest-fidelity plasma model. Developing numerical algorithms to solve these more complete plasma models that exploit the different physics offers computationally efficient methods that maintain high order spatial accuracy. The methods have been extend to other continuum descriptions, such as continuum kinetic plasma model and single-fluid MHD models. Combining the constituent plasma descriptions into a domain-hybridized model that solves a different plasma model in different portions of the domain produces numerical simulations with high physical fidelity with minimal computational cost. Next steps would include refining the constituent plasma models and improving the coupling throughout the computational domain. Additional improvements would include a dynamic adaptivity that adjusts the domain decomposition as the simulation evolves. The algorithm developed in the project, its implementation into WARPXM, and its application to benchmark and real experimental problems have demonstrated the capability of both the multi-fluid plasma model and the numerical techniques in the algorithm.

Acknowledgment/Disclaimer

This work was sponsored by the Air Force Office of Scientific Research, USAF, under grant number FA9550-15-1-0271. The views and conclusions contained herein are those of the author and should not be interpreted as necessarily representing the official policies or endorsements, either expressed or implied, of the Air Force Office of Scientific Research or the U. S. Government.

References

[1] A. Ho, I. A. M. Datta, and U. Shumlak. Physics-based-adaptive plasma model for high-fidelity numerical simulations. *Frontiers in Physics*, 6:105, 2018.

[2] S. T. Miller and U. Shumlak. A multi-species 13-moment model for moderately collisional plasmas. *Physics of Plasmas*, 23(8):082303, 2016.

[3] U. Shumlak, R. Lilly, N. Reddell, E. Sousa, and B. Srinivasan. Advanced physics calculations using a multi-fluid plasma model. *Computer Physics Communications*, 182(9):1767–1770, 2011.

[4] G. V. Vogman, U. Shumlak, and P. Colella. Conservative fourth-order finite-volume Vlasov–Poisson solver for axisymmetric plasmas in cylindrical (r, v_r, v_θ) phase space coordinates. *Journal of Computational Physics*, 373:877 – 899, 2018.

[5] E.M. Sousa and U. Shumlak. A blended continuous–discontinuous finite element method for solving the multi-fluid plasma model. *Journal of Computational Physics*, 326:56 – 75, 2016.

[6] C. Z. Cheng and Georg Knorr. The Integration of the Vlasov Equation in Configuration Space. *Journal of Computational Physics*, 22(3):330–351, 1976.

[7] H Ruhl and P Mulser. Relativistic Vlasov Simulation of Intense fs Laser Pulse-Matter Interactions Laser Pulse-Matter Interaction. *Physics Letters A*, 205(5-6):388–392, 1995.

[8] L. Chacon, D. C. Barnes, D. A. Knoll, and G. H. Miley. An implicit energy-conservative 2D Fokker-Planck algorithm. *Journal of Computational Physics*, 157(2):618–653, 2000.

[9] L. Chacon, D. C. Barnes, D. A. Knoll, and G. H. Miley. An implicit energy-conservative 2D Fokker-Planck algorithm - II. Jacobian-free Newton-Krylov solver. *Journal of Computational Physics*, 157(2):654–682, 2000.

[10] Y. Matsunaga, T. Hatori, and T. Kato. Kinetic simulation of nonlinear phenomena of an ion acoustic wave in gas discharge plasma with convective scheme. *Physics of Plasmas*, 8(3):1057–1069, 2001.

[11] M. H. L. van der Velden, W. J. M. Brok, J. J. A. M. van der Mullen, and V. Banine. Kinetic simulation of an extreme ultraviolet radiation driven plasma near a multilayer mirror. *Journal of Applied Physics*, 100(7):073303, 2006.

[12] Sanae-I Itoh and Kimitaka Itoh. Kinetic Description of Nonlinear Plasma Turbulence. *Journal Of The Physical Society Of Japan*, 78(12):124502, 2009.

[13] M. J. Keskinen. Fully Kinetic Fokker-Planck Model of Thermal Smoothing in Nonuniform Laser-Target Interactions. *Physical Review Letters*, 103(5):055001, 2009.

[14] D. Loffhagen and F. Sigeneger. Advances in Boltzmann equation based modeling of discharge plasmas. *Plasma Sources Science & Technology*, 18(3):034006, 2009.

[15] V. Guerra, K. Kutasi, M. Lino da Silva, P. A. Sa, and J. Loureiro. Kinetic Simulation of Discharges and After-Glows in Molecular Gases. *High Temperature Material Processes*, 14(1-2):141–156, 2010.

[16] G. V. Vogman, P. Colella, and U. Shumlak. Dory–Guest–Harris instability as a benchmark for continuum kinetic Vlasov–Poisson simulations of magnetized plasmas. *Journal of Computational Physics*, 277(0):101 – 120, 2014.

[17] C. K. Birdsall and A. B. Langdon. *Plasma Physics via Computer Simulation*. McGraw-Hill, New York, 1985.

[18] Zhang-Hu Hu, Yuan-Hong Song, and You-Nian Wang. Wake effect and stopping power for a charged ion moving in magnetized two-component plasmas: Two-dimensional particle-in-cell simulation. *Physical Review E*, 82(2-1):026404, 2010.

[19] C. Soria-Hoyo, F. Pontiga, and A. Castellanos. A PIC based procedure for the integration of multiple time scale problems in gas discharge physics. *Journal of Computational Physics*, 228(4):1017–1029, 2009.

[20] A. Stockem, M. E. Dieckmann, and R. Schlickeiser. PIC simulations of the temperature anisotropy-driven Weibel instability: analysing the perpendicular mode. *Plasma Physics And Controlled Fusion*, 52(8):085009, 2010.

[21] S. E. Parker and W. W. Lee. A fully nonlinear characteristic method for gyrokinetic simulation. *Physics of Fluids B - Plasma Physics*, 5(1):77–86, 1993.

[22] Manuel Torrilhon. Hyperbolic Moment Equations in Kinetic Gas Theory Based on Multi-Variate Pearson-IV-Distributions. *Communications in Computational Physics*, 7(4):639–673, 2010.

[23] U. Shumlak and J. Loverich. Approximate Riemann solver for the two-fluid plasma model. *Journal of Computational Physics*, 187(2):620–638, 2003.

[24] Jeffrey P. Freidberg. *Ideal Magnetohydrodynamics*. Plenum Press, New York and London, 1987.

[25] S. I. Braginskii. Transport processes in a plasma. In M. A. Leontovich, editor, *Reviews of Plasma Physics*, volume 1, pages 205–311. Consultants Bureau, New York, NY, 1965.

[26] S. Chapman and T. G. Cowling. *The Mathematical Theory of Non-Uniform Gases*. Cambridge University Press, Cambridge, 1939.

[27] J. D. Ramshaw. A Method for Enforcing the Solenoidal Condition on Magnetic Field in Numerical Calculations. *Journal of Computational Physics*, 52(3):592–596, 1983.

[28] C. D. Munz, P. Ommes, and R. Schneider. A three-dimensional finite volume solver for the Maxwell equations with divergence cleaning on unstructured meshes. *Computer Physics Communications*, 130:83–117, 2000.

[29] B. Marder. A method for incorporating Gauss' law into electromagnetic PIC codes. *Journal of Computational Physics*, 68(1):48–55, 1987.

[30] H. Grad. On the Kinetic Theory of Rarefied Gases. *Communications On Pure And Applied Mathematics*, 2(4):331–407, 1949.

[31] V. M. Zhdanov and G. A. Tirskii. The use of the moment method to derive the gas and plasma transport equations with transport coefficients in higher-order approximations. *PMM Journal of Applied Mathematics and Mechanics*, 67(3):365–388, 2003.

[32] R. Lilly and U. Shumlak. Comparisons of the two-fluid, ten moment and the two-fluid, five moment plasma models. *Bulletin of the American Physical Society*, 53(14), 2008.

[33] R. Lilly and U. Shumlak. Regions of validity for the 10-moment, two fluid plasma model. *DoD HPCMP Users Group Conference, 2008. DOD HPCMP UGC*, pages 150–153, 2008.

[34] Ammar Hakim. Extended MHD modeling with the ten-moment equations. *Journal of Fusion Energy*, 27(1-2):36–43, 2008.

[35] O. S. Jones, U. Shumlak, and D. S. Eberhardt. An implicit scheme for nonideal magnetohydrodynamics. *Journal of Computational Physics*, 130(2):231 – 242, 1997.

[36] A. Hakim, J. Loverich, and U. Shumlak. A high resolution wave propagation scheme for ideal two-fluid plasma equations. *Journal of Computational Physics*, 219(1):418 – 442, 2006.

[37] J. Loverich and U. Shumlak. A discontinuous Galerkin method for the full two-fluid plasma model. *Computer Physics Communications*, 169(1-3):251–255, 2005.

[38] J. Loverich, A. Hakim, and U. Shumlak. A discontinuous Galerkin method for ideal two-fluid plasma equations. *Communications in Computational Physics*, 9:240–268, 2011.

[39] B. Srinivasan, A. Hakim, and U. Shumlak. Numerical methods for two-fluid dispersive fast MHD phenomena. *Communications in Computational Physics*, 10:183–215, 2011.

[40] A. Hakim and U. Shumlak. Two-fluid physics and field-reversed configurations. *Physics of Plasmas*, 14(5):055911, 2007.

[41] J. Loverich and U. Shumlak. Nonlinear full two-fluid study of $m = 0$ sausage instabilities in an axisymmetric Z pinch. *Physics of Plasmas*, 13(8):082310, 2006.

[42] B. Srinivasan and U. Shumlak. Analytical and computational study of the ideal full two-fluid plasma model and asymptotic approximations for Hall-magnetohydrodynamics. *Physics of Plasmas*, 18(9):092113, 2011.

[43] E. T. Meier, A. H. Glasser, V. S. Lukin, and U. Shumlak. Modeling open boundaries in dissipative MHD simulation. *Journal of Computational Physics*, 231(7):2963 – 2976, 2012.

[44] E. Kansa, U. Shumlak, and S. Tsynkov. Discrete Calderon's projections on parallelepipeds and their application to computing exterior magnetic fields for FRC plasmas. *Journal of Computational Physics*, 234(0):172–198, 2013.

[45] E. T. Meier, V. S. Lukin, and U. Shumlak. Spectral element spatial discretization error in solving highly anisotropic heat conduction equation. *Computer Physics Communications*, 181(5):837–841, 2010.

[46] B. Cockburn and C. W. Shu. The Runge-Kutta discontinuous Galerkin method for conservation laws. *Journal of Computational Physics*, 141(2):199–224, 1998.

[47] Charles Hirsch. *Numerical Computation of Internal and External Flows*, volume 1. Butterworth-Heinemann, Oxford, United Kingdom, 2 edition, 2007.

[48] Petr Cagas, Ammar Hakim, James Juno, and Bhuvana Srinivasan. Continuum kinetic and multi-fluid simulations of classical sheaths. *Physics of Plasmas*, 24(2):022118, 2017.